Int. J. Appl. Math. Comput. Sci., 2009, Vol. 19, No. 3, 469–483
DOI: 10.2478/v10006-009-0038-y

amcs

AN OBJECT-ORIENTED APPROACH TO SIMULATING HUMAN GAIT MOTION BASED ON MOTION TRACKING

MARTIN TÄNDL *, TOBIAS STARK *, NIHAT ERCÜMET EROL **, FRANZ LÖER **, ANDRÉS KECSKEMÉTHY *

* Department of Mechanical and Process Engineering
University of Duisburg-Essen, Lotharstraße 1, 47057 Duisburg, Germany
e-mail: andres.kecskemethy@uni-due.de

** Department of Orthopaedics
Universitätsklinikum Essen, Hufelandstraße 55, 45147 Essen, Germany
e-mail: nihat.erol@rub.de, franz.loeer@uni-essen.de

Accurate bone motion reconstruction from marker tracking is still an open and challenging issue in biomechanics. Presented in this paper is a novel approach to gait motion reconstruction based on kinematical loops and functional skeleton features extracted from segmented Magnetic Resonance Imaging (MRI) data. The method uses an alternative path for concatenating relative motion starting at the feet and closing at the hip joints. From the evaluation of discrepancies between predicted and geometrically identified functional data, such as hip joint centers, a cost function is generated with which the prediction model can be optimized. The method is based on the object-oriented multibody library MOBILE, which has already been successfully applied to the development of industrial virtual design environments. The approach has been implemented in a general gait visualization environment termed *Mobile Body*.

Keywords: gait/motion analysis, muskuloskeletal system, multibody simulation, MRI, X-ray, motion tracking.

1. Introduction

Human motion analysis has gained significant importance over the last years in different areas such as medicine, entertainment industry, and sports. It involves three main steps, namely, the capturing of motion, the processing of the captured data upon appropriate kinematic modeling, and the final interpretation of the information delivered by the model.

There exist various approaches regarding motion capturing techniques: video camera recording, the measurement of accelerations at each of the moving bodies, and optical marker-based motion tracking. The limitations and advantages of these techniques have been studied extensively, as shown, for example, in (Maestri, 1995; Peters *et al*., 2009; Zordan and Van Der Horst, 2003; Barbour and Schmidt, 2001). Hereby, motion tracking via marker recognition still features a number of advantages, such as high precision, a high sampling rate, and a high number of tractable bodies, which is the reason why it is still used quite frequently in practice.

In this paper, an improved procedure for motion tracking of human gait based on markers and infrared cameras is presented. The core component is an object-oriented mechanical model of the musculoskeletal system, which uses higher concepts from kinematics, such as closed loops and the interpolation of rotation axes, and offers an open-architecture software environment for easy coupling of the model with sensor devices and 3D interactive rendering. The mechanical model is built using the object-oriented multibody library MOBILE, has also been applied to other mechanical system, (e.g., robots, satellites, vehicles, and complex industrial equipment). For the underlying kinematical skeleton, several approaches have been proposed in the literature, such as (Oxford Metrics, 2004; Delp and Loan, 2000). In these models, the kinematical chains typically start at the hip (as the root) and propagate through the thighs, knees and shanks to the feet (as leaves). This has the disadvantage that the first reference system from which the chains propagate is already quite blurred due to artifacts generated from skin and soft tissue motion between markers and pelvis at the hip (Della Croce *et al*., 2005). To overcome

this difficulty, in this paper a different procedure is proposed, in which the kinematic chains start at the feet and propagate towards the hip, where a closed loop is generated. Using this information, more precise predictions of knee axes are possible, as the artifacts at the feet and the shank are smaller than those at the hip. An additional improvement of motion tracking accuracy is obtained by using data fusion techniques for combining geometric information gained from segmented MRI bone data with motion data obtained from gait measurements. Thus errors from motion tracking can be reduced and a more accurate motion model is obtained which can be used for further analysis or medical prediction.

The rest of the paper is organized as follows: Section 2 describes the basic components with which a mechanical model can be built using the object-oriented multibody library MOBILE. In Section 3, the underlying kinematical model of the legs as well as a new foot-contact model for interactions between feet and ground are presented. Section 4 describes the data fusion techniques used to amalgamate MRI segmentation data with the kinematical models restored from motion tracking data. Finally, in Section 5 some validation results are presented, showing that the proposed model yields more accurate results.

2. Object-oriented multibody simulation library MOBILE

The core component of the integrated simulation system is the mechanical model of the musculoskeletal system. Its implementation using object-oriented programming makes it easy to combine it with an image processing code, visualization libraries and libraries for reading/writing files containing the model parameters. In the present setting, the multibody library MOBILE is employed for this purpose, and it offers the possibility of starting with simple model components, and refining and replacing these with more complex elements as needed on a case-by-case basis. These may be individual models of anatomical joints of special interest or tailored analysis modules for clinical application. In this section, the main concepts of the MOBILE programming environment are presented for better reference. More detailed descriptions can be found in (Kecskeméthy and Hiller, 1994a).

2.1. Concept of kinetostatic transmission elements. In MOBILE, mechanical components are modeled as abstract mappings, termed *kinetostatic transmission elements*, which transmit motion and loads between sets of input and output variables called *state objects*. In this way, any mechanical model can be assembled by concatenating these kinetostatic transmission elements as parts of the real system. Since MOBILE is implemented using the object-oriented programming language C++, new elements can be added easily using the concept of inheritance (Stroustrup, 1991).

Mathematically, the operations related to kinetostatic transmission elements correspond to well-known mappings of differential geometry: the transmission of position and velocity correspond to a nonlinear mapping between two smooth manifolds, and the corresponding *push-forward* function for tangent vectors, respectively, while the force mapping corresponds to the *pull-back* function being applied to cotangent vectors. From the computational point of view, the concept renders a *responsibility-driven client/server* model (Wirfs-Brock and Wilkerson, 1989), in which multibody operations are defined as "services" that an object provides at any time during program execution independently of its internal implementation according to a specific "contract". In the present mechanical modeling, the basic "contract" of kinetostatic transmission elements consists of two main services: one for the transmission of motion and one for the transmission of forces.

As displayed in Fig. 1, a mechanical component is regarded as a map from a set of n variables collected in the *input vector* $\boldsymbol{q}$ to a set of m variables collected in the *output vector* $\boldsymbol{q}'$.

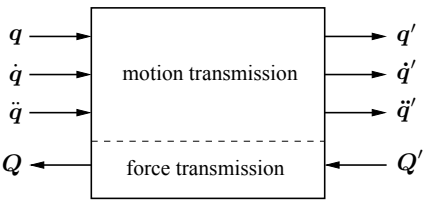

Fig. 1. Simple model of a kinetostatic transmission element.

Associated with this mapping, there exist three kinematic functions and one force-associated function. The kinematic functions are the mapping itself and its first and second derivatives. These are collected in the *motion transmission functions*:

$$\left.\begin{array}{ll} \underline{\text{position:}} & \boldsymbol{q}' = \boldsymbol{\varphi}\,(\,\boldsymbol{q}\,) \\ \underline{\text{velocity:}} & \dot{\boldsymbol{q}}' = \mathbf{J}_\phi\,\dot{\boldsymbol{q}} \\ \underline{\text{acceleration:}} & \ddot{\boldsymbol{q}}' = \mathbf{J}_\phi\,\ddot{\boldsymbol{q}} + \dot{\mathbf{J}}_\phi\,\dot{\boldsymbol{q}} \end{array}\right\}. \qquad (1)$$

Here, $\mathbf{J}_\phi = \partial\boldsymbol{\varphi}/\partial\boldsymbol{q}$ is the $m \times n$ *Jacobian* of the transmission element, which is not required explicitly by the clients of the `MoMap` element. For the *force transmission function*, one assumes that the transmission element is *ideal*, i.e., that it neither consumes nor produces power. Then, virtual work at the input and output are equal:

$$\delta\boldsymbol{q}^{\mathrm{T}}\,\boldsymbol{Q} = \delta\boldsymbol{q}'^{\mathrm{T}}\,\boldsymbol{Q}'. \qquad (2)$$

After substituting $\delta\boldsymbol{q}' = \mathbf{J}_\phi\,\delta\boldsymbol{q}$ and noting that this condition must hold for all $\delta\boldsymbol{q} \in \mathbf{R}^n$, one obtains

$$\underline{\text{force:}} \qquad \boldsymbol{Q} = \mathbf{J}_\phi^{\mathrm{T}}\,\boldsymbol{Q}', \tag{3}$$

where $\mathbf{J}_\phi^{\mathrm{T}}$ denotes the transpose of the Jacobian $\mathbf{J}_\phi$. Note that this transformation is directed from the (kinematical) output of the transmission element to its (kinematical) input. Note also that, in general, $\mathbf{J}_\phi$ does not need to be regular, in fact, not even quadratic, so one cannot assume that (3) can be inverted. Thus force transmission is in general routed in the *opposite* direction to motion transmission.

In MOBILE, kinetostatic transmission elements can be concatenated by connecting the outputs of one element to the inputs of the other. The transmission functions of such a composite transmission element can be realized by the concatenation of motion transmission in order of the mechanical chain starting at the root of the chain and in reverse order for force transmission. Inputs and outputs of transmission elements can be scalar or spatial quantities. They are regarded in MOBILE as *state objects*. Spatial motion is stored in *frames* $\mathcal{K}$, while scalar quantities are stored in objects termed *scalar variables* β. Each of these objects embraces complete information regarding position, velocity, acceleration and load. In MOBILE, each frame is represented by an individual state object with members $\mathbf{R}$, $\boldsymbol{r}$, $\boldsymbol{\omega}$, $\boldsymbol{v}$, $\dot{\boldsymbol{\omega}}$, $\boldsymbol{a}$, $\boldsymbol{\tau}$, $\boldsymbol{f}$ denoting the rotation matrix, the radius vector, the angular and linear velocity vectors, the angular and linear acceleration vectors, the torque and the force, respectively. As a convention, all vectors are assumed to be decomposed in the moving frame $\mathcal{K}$. Scalar state objects in MOBILE have members β, $\dot{\beta}$, $\ddot{\beta}$, Q_β denoting position, velocity, acceleration, and generalized force of the variable. State objects act as interface elements between which the kinetostatic transmission elements carry out their mappings: frames represent the junctions by which the mechanical components are connected together, while scalar state objects represent the actuator variables which are used to drive the joints or to move the bodies along a prescribed trajectory.

Below we describe the basic transmission elements used for biomechanical modeling of human gait.

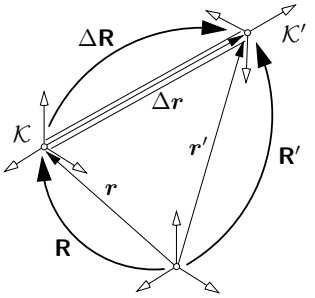

Fig. 2. Mechanical model of a rigid link.

2.2. Rigid links. A rigid link (Fig. 2) describes the motion of an output frame $\mathcal{K}'$ that is rigidly connected to the input frame $\mathcal{K}$. Let the relative position and orientation of the output frame be described by the offset vector $\Delta\boldsymbol{r}$ and the rotation matrix $\Delta\mathbf{R}$, respectively. Then, the corresponding motion transmission functions are

$$\mathbf{R}' = \mathbf{R}\cdot\Delta\mathbf{R},$$
$$\boldsymbol{r}' = \Delta\mathbf{R}^{\mathrm{T}}\,\boldsymbol{r} + \Delta\boldsymbol{r}, \tag{4}$$
$$\begin{bmatrix} \boldsymbol{\omega}' \\ \boldsymbol{v}' \end{bmatrix} = \mathbf{J}_\phi \begin{bmatrix} \boldsymbol{\omega} \\ \boldsymbol{v} \end{bmatrix}, \tag{5}$$
$$\begin{bmatrix} \dot{\boldsymbol{\omega}}' \\ \boldsymbol{a}' \end{bmatrix} = \mathbf{J}_\phi \begin{bmatrix} \dot{\boldsymbol{\omega}} \\ \boldsymbol{a} \end{bmatrix} + \begin{bmatrix} 0 \\ \boldsymbol{\omega}'\times(\boldsymbol{\omega}'\times\Delta\boldsymbol{r}) \end{bmatrix} \tag{6}$$

for pose, velocity, and acceleration, where

$$\mathbf{J}_\phi = \begin{bmatrix} \Delta\mathbf{R}^{\mathrm{T}} & 0 \\ -\widetilde{\Delta\boldsymbol{r}}\,\Delta\mathbf{R}^{\mathrm{T}} & \Delta\mathbf{R}^{\mathrm{T}} \end{bmatrix} \tag{7}$$

and

$$\widetilde{\Delta\boldsymbol{r}} = \begin{bmatrix} 0 & -\Delta\boldsymbol{r}_z & \Delta\boldsymbol{r}_y \\ \Delta\boldsymbol{r}_z & 0 & -\Delta\boldsymbol{r}_x \\ -\Delta\boldsymbol{r}_y & \Delta\boldsymbol{r}_x & 0 \end{bmatrix}. \tag{8}$$

The force transmission is obtained by the transposed Jacobian as

$$\begin{bmatrix} \boldsymbol{\tau} \\ \boldsymbol{f} \end{bmatrix} = {\mathbf{J}_\phi}^{\mathrm{T}} \begin{bmatrix} \boldsymbol{\tau}' \\ \boldsymbol{f}' \end{bmatrix}. \tag{9}$$

In the context of biomechanical simulation, rigid links are used to model bony structure and to define functional items of the bone, such as joint and muscle origins, via insertion points for muscles and tendons, or bone shaft and transversal axes, respectively.

2.3. Elementary joints. Anatomical joints involve complex surface-surface contacts and additional tendon constraints. In biomechanical modeling, they are represented by surrogate mechanisms (Parenti-Castelli *et al.*, 2004; Kecskeméthy and Weinberg, 2003) or by simple joint-like spherical pairs. An example of an elementary

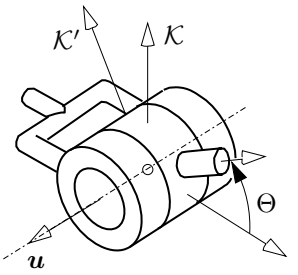

Fig. 3. Mechanical model of a revolute joint.

joint is the revolute joint shown in Fig. 3. The transmission functions are

$$\mathbf{R}' = \mathbf{R} \cdot \Delta\mathbf{R}, \;\; \Delta\mathbf{R} = \mathtt{Rot}\,[\boldsymbol{u}, \Theta\,],$$
$$\boldsymbol{r}' = \Delta\mathbf{R}^{\mathrm{T}}\,\boldsymbol{r}, \tag{10}$$

$$\begin{bmatrix} \boldsymbol{\omega}' \\ \boldsymbol{v}' \end{bmatrix} = \mathbf{J}_\phi \begin{bmatrix} \boldsymbol{\omega} \\ \boldsymbol{v} \\ \dot\Theta \end{bmatrix}, \tag{11}$$

$$\begin{bmatrix} \dot{\boldsymbol{\omega}}' \\ \boldsymbol{a}' \end{bmatrix} = \mathbf{J}_\phi \begin{bmatrix} \dot{\boldsymbol{\omega}} \\ \boldsymbol{a} \\ \ddot\Theta \end{bmatrix} + \begin{bmatrix} \boldsymbol{\omega}' \times \boldsymbol{u}\,\dot\Theta \\ 0 \end{bmatrix}$$

for the motion from $\mathcal{K}$ to $\mathcal{K}'$, and

$$\begin{bmatrix} \boldsymbol{\tau} \\ \boldsymbol{f} \\ Q_\Theta \end{bmatrix} = \mathbf{J}_\phi^{\mathrm{T}} \begin{bmatrix} \boldsymbol{\tau}' \\ \boldsymbol{f}' \end{bmatrix}, \tag{12}$$

where

$$\mathbf{J}_\phi = \begin{bmatrix} \Delta\mathbf{R}^{\mathrm{T}} & 0 & \boldsymbol{u} \\ -\widetilde{\Delta\boldsymbol{r}}\,\Delta\mathbf{R}^{\mathrm{T}} & \Delta\mathbf{R}^{\mathrm{T}} & 0 \end{bmatrix}, \tag{13}$$

for the forces at the output $\boldsymbol{\tau}'$, $\boldsymbol{f}'$ to the forces at the input $\boldsymbol{\tau}$, $\boldsymbol{f}$ and the moment Q_Θ along the joint axis $\boldsymbol{u}$.

Other joints with more complex kinematics can be incorporated easily, substituting the internal transmission functions of the elementary model of the revolute joint while keeping the overall structure intact.

2.4. Mass elements. Mass and inertia of biomechanical body parts are modeled as mass elements whose mechanical model is shown in Fig. 4. The mass element com-

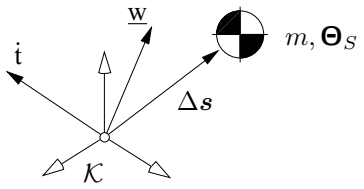

Fig. 4. Mechanical model of the mass and inertia of a rigid body.

putes the d'Alembert forces

$$\boldsymbol{f} \;=\; -m\Big[\boldsymbol{a} + \dot{\boldsymbol{\omega}} \times \Delta\boldsymbol{s} + \boldsymbol{\omega} \times (\boldsymbol{\omega} \times \Delta\boldsymbol{s})\Big], \tag{14}$$

$$\boldsymbol{\tau} \;=\; -\Big[\mathbf{\Theta}_S\,\dot{\boldsymbol{\omega}} + \boldsymbol{\omega} \times \mathbf{\Theta}_S\,\boldsymbol{\omega}\Big] + \Delta\boldsymbol{s} \times \boldsymbol{f}, \tag{15}$$

acting on the body-fixed frame $\mathcal{K}$ as functions of the mass m, the inertia tensor with respect to the center of mass $\mathbf{\Theta}_S$, the offset of the center of mass $\Delta\boldsymbol{s}$, the input accelerations $\dot{\boldsymbol{\omega}}$, $\boldsymbol{a}$, and the angular velocity $\boldsymbol{\omega}$ of frame $\mathcal{K}$. For compact notation, the angular and linear velocities are combined to a twist t the moment and the force on the frame form a wrench $\underline{\mathrm{w}}$.

2.5. Measurement objects. A further set of elements introduced in M[]BILE to model mechanical structures are measurement or "chord" objects. A chord object takes some state objects and projects their state to some other variables (in general scalar variables), termed "measures". For biomechanical modeling, the linear distance between two points (origins of frames) plays a fundamental role in representing muscles and tendons.

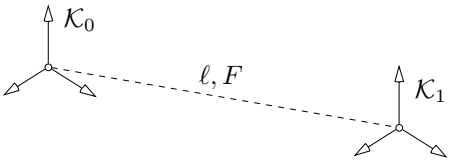

Fig. 5. Measurement of the distance between two frame origins.

In the motion transmission mode, the linear distance chord computes the distance between the origins of two frames $\mathcal{K}_0$ and $\mathcal{K}_1$, as well as its time derivatives, respectively:

$$\ell \;=\; \|\,\boldsymbol{d}\,\| \quad \text{with} \quad \boldsymbol{d} = \mathbf{R}_1\,\boldsymbol{r}_1 - \mathbf{R}_0\,\boldsymbol{r}_0, \tag{16}$$

$$\dot\ell \;=\; \underbrace{\left[0\,,\; \frac{\boldsymbol{d}^{\mathrm{T}}}{\|\,\boldsymbol{d}\,\|}\mathbf{R}_1\,,\; 0\,,\; -\frac{\boldsymbol{d}^{\mathrm{T}}}{\|\,\boldsymbol{d}\,\|}\mathbf{R}_0\right]}_{\mathbf{J}_\phi} \begin{bmatrix} \boldsymbol{\omega}_\ell \\ \boldsymbol{v}_\ell \\ \boldsymbol{\omega}_r \\ \boldsymbol{v}_r \end{bmatrix}, \tag{17}$$

$$\ddot\ell \;=\; \mathbf{J}_\phi \begin{bmatrix} \dot{\boldsymbol{\omega}}_\ell \\ \boldsymbol{a}_\ell \\ \dot{\boldsymbol{\omega}}_r \\ \boldsymbol{a}_r \end{bmatrix} + \frac{(\mathbf{R}_1\,\boldsymbol{v}_\ell - \mathbf{R}_0\,\boldsymbol{a}_r)}{\ell} - \frac{\dot\ell^2}{\ell}. \tag{18}$$

Conversely, in the force transmission mode, the chord object projects the tension F in the chord to the forces at the attached frames:

$$[\,\boldsymbol{\tau}_\ell,\, \boldsymbol{f}_\ell,\, \boldsymbol{\tau}_r,\, \boldsymbol{f}_r\,]^{\mathrm{T}} = \mathbf{J}_\phi^{\mathrm{T}} F. \tag{19}$$

2.6. Chains of linear chords. Muscles often span several via points, which must be modeled appropriately. In the M[]BILE environment, such situations can be easily represented by a concatenation of elementary linear measurements connecting a series of frames $\mathcal{K}_1, \ldots \mathcal{K}_{n-1}$ (Fig. 6). The motion transmission for such a chain of n linear chords is then

$$\ell = \sum_{i=1}^{n} \ell_i, \tag{20}$$

$$\dot\ell = \underbrace{[\,1, \ldots, 1\,]}_{\mathbf{J}_\phi}\,\dot{\boldsymbol{q}}, \tag{21}$$

$$\ddot\ell = \mathbf{J}_\phi\,\ddot{\boldsymbol{q}}, \tag{22}$$

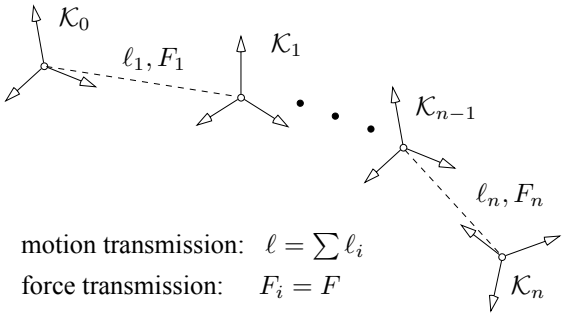

Fig. 6. Measurement of the length of a polygon line spanned by frame origins.

where $\boldsymbol{q} = [\ell_1, \ldots, \ell_n]^{\mathrm{T}}$ embodies the lengths of individual chords. Correspondingly, assuming frictionless guidance of the muscles, the force transmission is simply

$$\underline{\text{force:}} \qquad \boldsymbol{Q} = \mathbf{J}_{\phi}^{\mathrm{T}}\, F, \tag{23}$$

meaning that the forces $\boldsymbol{Q} = [F_1\,,\, F_2\,,\, \ldots\,,\, F_n]^{\mathrm{T}}$ at the individual linear chords are all equal to a common value F.

2.7. Objects for the closure of loops. Multibody systems can feature two fundamental types of structure: (i) tree-type or open structures and (ii) closed-loop structures. In biomechanics, mostly the body is considered as a tree-type structure starting at the torso and propagating to the distal limbs (hands, feet, head). However, in some cases, as shown in this paper, it may be convenient to start at the limbs and continue to the torso, which creates ambiguity that must be thus forced to concurrence by constraint functions. These constraint functions generate topologically closed loops, which must be solved by appropriate constraint solvers.

In MOBILE, the closure of loops is accomplished as a two-stage process. In a first stage, a set of characteristics is defined whose vanishing indicates the closure of the loop. These measurements are typically generalized distances between geometric elements such as points, planes and lines. MOBILE provides, apart from the linear measurement object described above, a whole family of classes for making such measurements. In the second stage, one or more objects termed "*solvers*" are defined that are set to determine the dependent relative motions within the loop such that the measurements vanish. MOBILE supplies two classes for this purpose, which are both derived from the (abstract) super-class *MoSolver*. One solves the constraint equations by iterative, Newton-based procedures. This is the universal, generally applicable method. The other takes a scalar equation and solves it in a *closed form* for an unknown joint variable. This method only works for special types of measurements and loop architectures. In both cases, the resulting solver objects behave again like kinetostatic transmission elements, supplying a motion and force transmission function.

In the present biomechanics modeling, such constraint solvers are used to force the matching of pelvis functional points obtained from the two leg chains starting at the feet.

3. Kinematical and dynamic gait model

In this chapter, the mechanical model used to reproduce human motion is described in greater detail. The description begins with the overall definition of the forward and inverse dynamics models, and then it specifies the special kinematical chains used to improve motion reproduction based on marker tracking.

3.1. Basic multibody model. Figure 7 shows the right side of the multibody model of the lower body that consists of seven rigid parts (torso, thighs, calves and feet) linked by ideal joints. The torso represents the upper part of the body including head and arms assumed to be in rest with respect to the torso. Its pose is described by

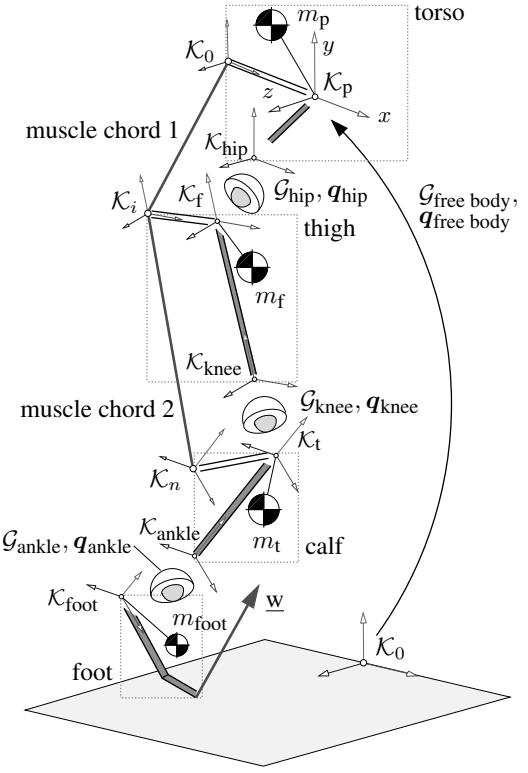

Fig. 7. Multibody model of the lower body (right leg).

the pelvis-fixed reference frame $\mathcal{K}_{\mathrm{p}}$, which is guided by the free-body joint $\mathcal{G}_{\text{free body}}$ with six joint coordinates

$\boldsymbol{q}_{\text{free body}}$ (the three Cartesian coordinates of the origin of $\mathcal{K}_\text{p}$ as well as the three Bryant angles describing the rotation angles for a rotation sequence about the z, y and x axes, respectively, in that order). The thighs are connected to the torso via hip joints $\mathcal{G}_\text{hip}$ between the pelvis-fixed frame $\mathcal{K}_\text{hip}$ and the femur reference frame $\mathcal{K}_\text{f}$. The hip joints are modeled by a chain of three revolute joints with pairwise perpendicular axes, rendering a Bryant-angle parameterization of the spherical joint with angles $\boldsymbol{q}_\text{hip}$ corresponding to the flexion, adduction and axial rotation in the joint.

The same parameterization is used for the knee joint $\mathcal{G}_\text{knee}$ connecting the distal femur frame $\mathcal{K}_\text{knee}$ to the tibia frame $\mathcal{K}_\text{t}$ as well as the ankle joint $\mathcal{G}_\text{ankle}$ between the frames $\mathcal{K}_\text{ankle}$ and $\mathcal{K}_\text{foot}$. All joint coordinates ($\boldsymbol{q}_{\text{free body}}$, $\boldsymbol{q}_\text{hip}$ as well as $\boldsymbol{q}_\text{knee}$, $\boldsymbol{q}_\text{ankle}$ for both legs) are combined into the vector $\boldsymbol{q}$ of $f = 24$ generalized coordinates of the complete system. The mass properties of the segments torso, thigh, calf, foot are represented by mass elements $\{m_\text{p}, \boldsymbol{\Theta}_{S,\text{p}}, \Delta\boldsymbol{s}_\text{p}\}$, $\{m_\text{f}, \boldsymbol{\Theta}_{S,\text{f}}, \Delta\boldsymbol{s}_\text{f}\}$, $\{m_\text{t}, \boldsymbol{\Theta}_{S,\text{t}}, \Delta\boldsymbol{s}_\text{t}\}$, and $\{m_\text{foot}, \boldsymbol{\Theta}_{S,\text{foot}}, \Delta\boldsymbol{s}_\text{foot}\}$, respectively. The kinematics of muscles are taken into account by chains of n chords measuring the length of the polygon line spanned from a body-fixed origin frame $\mathcal{K}_0$, possibly over via frames $\mathcal{K}_i$ to the insertion frame $\mathcal{K}_n$. Dynamic muscle models like the Hill-type muscle model (Hill, 1938) can be used to compute muscle forces that are applied to the rigid bodies via the force transmission function of the chord chain.

Note that only one muscle is displayed in Fig. 7, but arbitrarily many can be added to the multibody model used in the simulation environment. The ground reaction wrench $\underline{\text{w}}$ and its center of pressure are computed using measured force plate data and applied to the frame $\mathcal{K}_\text{foot}$ when analyzing experimental gait lab data. This system consists of a kinematical subsystem (joints and rigid links) as well as the attached mass and force elements and is regarded as one transmission element denominated *global kinematics*.

By prescribing the motion of the generalized coordinates $\boldsymbol{q}$, their time derivatives and the applied ground reaction forces, collected in a vector $\underline{\text{W}}^{(e)}$ and performing the composition of the motion and force transmission function, one obtains the function $\varphi_S^{D^{-1}}$ which implements exactly the *inverse dynamics* of the system, i.e., the computation of the *residual forces*

$$\begin{aligned}\overline{\boldsymbol{Q}} &= \varphi_S^{D^{-1}}(\,\boldsymbol{q}\,,\,\boldsymbol{q}\,,\,\ddot{\boldsymbol{q}}\,;\,\underline{\text{W}}^{(e)}\,;\,t\,)\\ &= -\mathbf{M}\,(\boldsymbol{q};t)\,\ddot{\boldsymbol{q}} - \widehat{\boldsymbol{Q}}\,(\,\boldsymbol{q}\,,\,\dot{\boldsymbol{q}}\,;\,\underline{\text{W}}^{(e)}\,;\,t).\end{aligned} \tag{24}$$

These residual forces $\overline{\boldsymbol{Q}}$ are the generalized forces at the free body joint $\mathcal{G}_{\text{free body}}$ and at the joints $\mathcal{G}_\text{hip}$, $\mathcal{G}_\text{knee}$, and $\mathcal{G}_\text{ankle}$, which lead to the motion given by $\boldsymbol{q}\,,\,\dot{\boldsymbol{q}}\,,\,\ddot{\boldsymbol{q}}$ for prescribed applied forces $\underline{\text{W}}^{(e)}$. In the present work, the joint coordinates $\boldsymbol{q}$ are estimated from the marker motion and the time derivatives $\dot{\boldsymbol{q}}$ and $\ddot{\boldsymbol{q}}$ are computed using widely used digital filtering (Winter, 1990) and numerical differentiation.

Conversely, as shown in (Kecskeméthy and Hiller, 1994b), the inverse dynamics can be used to built up the direct dynamics of the system by repeated evaluation of the residual forces for special kinematical inputs. Thus, both direct and inverse dynamics can be realized with the present model.

3.2. Foot-ground contact elements. In forward dynamics simulation of biomechanical motion, the reaction forces between foot and floor are to be determined as a function of the foot penetration. Presented here is a novel foot model consisting of two rigid segments (fore foot and hind foot) connected by a revolute joint with a nonlinear spring-damper element in parallel. As shown in Fig. 8, the input frame $\mathcal{K}$ of the foot element is fixed to the hind foot. Its origin is located at the center of the upper ankle joint, the z-axis is aligned with the axis of the ankle joint and the direction of the x-axis is chosen such that it is parallel to the ground in a neutral null position. The revolute joint connecting the hind foot to the fore foot is aligned with the z-axis and its position relative to the input frame is described by the vector $\Delta\boldsymbol{r}_3$. The contact between the foot and the ground is modeled with two regularized circle-plane contact elements as described by (Kecskeméthy *et al.*, 2000). One contact circle (radius R_2) is fixed to the hind foot at the position $\Delta\boldsymbol{r}_2$ parallel to the xz-plane of $\mathcal{K}$. The other contact circle is fixed to the fore foot (radius R_1, offset $\Delta\boldsymbol{r}_1$).

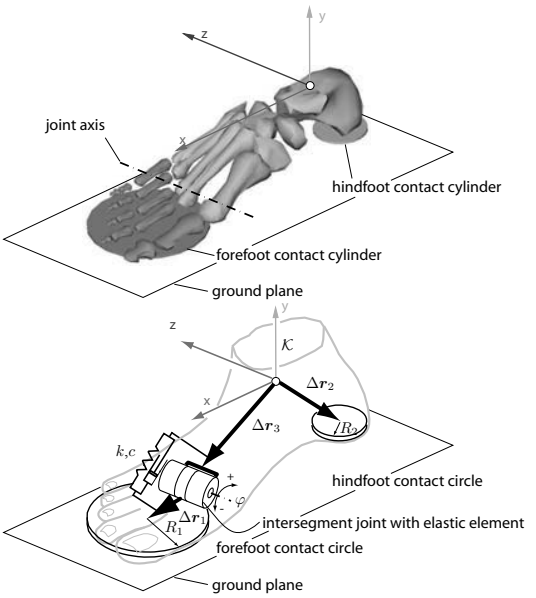

Fig. 8. Elastokinematic foot model with circle-plane contact pairs.

The unknown parameters of the contact elements are the intersegment revolute joint stiffness as well as the offset vectors $\Delta\boldsymbol{r}_1, \Delta\boldsymbol{r}_2$ and $\Delta\boldsymbol{r}_3$. These are collected in a 5×1 vector $\boldsymbol{x}$ of design parameters to be determined by an optimizing process described further below. For the identification procedure, one starts by measuring contact forces and foot positions at m discrete time points t_i. From these measured data, the corresponding wrench values $\underline{\mathrm{w}}_a(t_i)$ at the ankle joint are computed. The ankle joint wrench is applied to the input frame $\mathcal{K}$ of the foot element and the static equilibrium pose of the foot model under this load is determined for $i = 1, \ldots, m$. The pose at static equilibrium is parameterized by the global coordinates $\boldsymbol{r}_{\mathrm{sim},i}$ of the origin of the frame $\mathcal{K}$ and the Bryant angles (x, y and z rotation sequence) of $\mathcal{K}$, collected in $\boldsymbol{p}_{\mathrm{sim},i}$. These simulated values are compared to the measured pose values ($\boldsymbol{r}_{\mathrm{meas}}(t_i)$ and $\boldsymbol{p}_{\mathrm{meas}}(t_i)$), which are parameterized in the same way as the simulated ones. Parameter estimation is performed by minimizing the quadratic cost function

$$\mathrm{F}(\boldsymbol{x}) = \frac{1}{2}\sum_{i=1}^{m}\left[(\boldsymbol{r}_{\mathrm{meas}}(t_i) - \boldsymbol{r}_{\mathrm{sim},i})^2 + (\boldsymbol{p}_{\mathrm{meas}}(t_i) - \boldsymbol{p}_{\mathrm{sim},i})^2\right], \tag{25}$$

where $\boldsymbol{x}$ is the vector of unknown parameters of the foot model. Fig. 9 shows as an example of the identified parameters the measured and simulated rotation angle about the transversal axis, i.e., in the sagittal plane, between hind foot and ground. As can be seen, there is a fairly good qualitative matching between measurement and simulation, with a slight bias towards a tilt to the front for the simulated behavior. This difference is due to still not optimally identified model parameters such as the radius of the contact circles and the stiffness of the circle/plane penetration. However, for rough forward simulation purposes, a variation of 5° for this angle is acceptable, as it has no significant influence on the overall dynamic behavior.

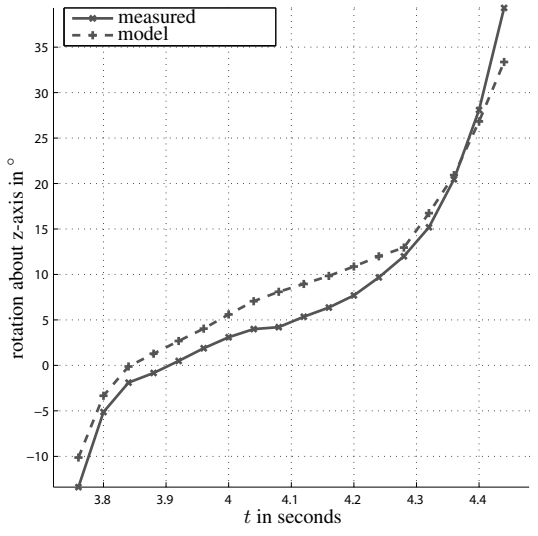

Fig. 9. Measured and simulated orientation of hind foot with identified parameters.

3.3. Segment motion estimation from marker movement. In the following, the problem of identifying the motion of the musculoskeletal system from the marker trajectories is discussed. To access the trajectories of the markers attached to the skin of a patient, we used the motion capturing system Vicon Nexus (`http://www.vicon.com`). The Vicon system consists of several infrared cameras and a measurement PC. The infrared light is reflected by the markers on the skin of the patient and then recorded by the cameras as two-dimensional images. From these images, the position in space of each marker is reconstructed at each camera frame, yielding the spatial trajectories of the markers as a function of time. The markers are associated with bony features stored in a *Plug-in-Gait* marker model contained in the Vicon analysis software Nexus (Vicon Motion Systems Limited, 2007). Figure 10(a) a shows the right leg with the markers used for this leg motion reconstruction model. For this model, a pelvis-fixed frame $\mathcal{K}_{\mathrm{p}}$ is defined using the hip markers RASI (right anterior superior iliac spine), LASI (left anterior superior iliac spine), RPSI (right posterior superior iliac spine), and LPSI (left posterior superior iliac spine), such that the z-axis is aligned with the line connecting the markers RASI and LASI and the centroid of RPSI and LPSI markers lies in the xz-plane. For the pelvis, the position of hip joint centers is estimated using the Newington-Gage model (Davis *et al.*, 1991) with the inter-ASI distance. The motion of the other leg segments is reconstructed starting at the hip joints, advancing down to the foot, sequentially computing new segment orientations using joint centers already determined and markers fixed to the next body part according to the algorithm described in (Vicon Motion Systems Limited, 2007).

A major problem encountered when using marker-based segment motion reconstruction is that due to errors resulting from inaccurate marker placement, skin motion at knee and ankle or soft tissue artifacts of the thigh marker (RTHI), wrong hip joint center positions and large (axial) rotations of tibia and femur can be encountered. These errors can be reduced by careful marker placement and by performing new measurements with improved marker positions, but this is hardly possible in routine measurements with patients. Thus, the predicted rotations, in particular about the longitudinal axis of femur and tibia, may be highly inaccurate.

Approaches to reducing these errors after the measurement has been carried out were presented, e.g.,

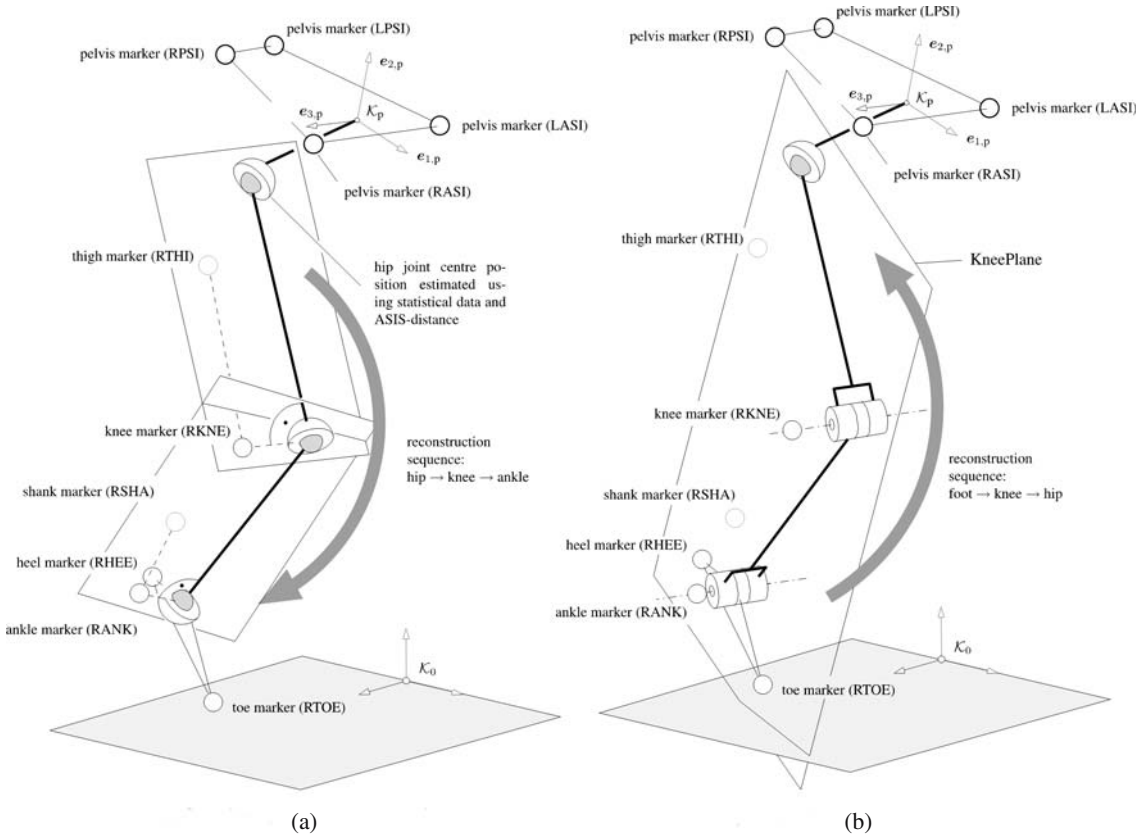

Fig. 10. Kinematic structure of the *Plug-in-Gait* model and the proposed model: (a) Vicon *Plug-in-Gait* model, (b) suggested kinematic model.

in (Cerveri *et al*., 2005) and (Kecskeméthy *et al*., 2003); the latter reduces model bone length variations by identifying the unknown constant offsets between the joint centers delivered by the motion capture system (prediction) and the anatomical joint centers.

The approach presented here is to compute the axes of the ankle joint and the knee joint starting at the foot markers, and proceeding upwards to the knee, using foot- and knee markers, which are subject to less (or at least more predictable) soft tissue motion. It is assumed that the ankle joint $\mathrm{R}_{\mathrm{ankle}}$ and the knee joint $\mathrm{R}_{\mathrm{knee}}$ are revolute joints. This restricts the application to gait motion with low knee flexion angles, since larger external/internal rotation (up to 37°) in the knee are possible for large flexion angles in (Piazza and Cavanagh, 2000). However, such extreme rotations do not appear in normal gait and can be included in future models without changing the overall procedure. Another assumption is that the line connecting the heel marker and the toe marker (unit vector $\boldsymbol{u}_{\mathrm{foot}}$) is perpendicular to both the ankle joint axis and the knee joint axis (Fig. 11(a)). An approximation of the hip joint center position is computed at the end of the procedure in such a way that the relative motion of one femur point with respect to the pelvis is minimized. The segment motion is determined with respect to an inertially fixed frame $\mathcal{K}_0$, usually coinciding with the reference frame of the motion capturing system. For describing vectors using Cartesian coordinate frames, the notation ${}_i^k\boldsymbol{b}_j$ is used, where k denotes the frame of decomposition, i denotes the frame with respect to which the motion is measured, and j denotes the target frame. For motions measured with respect to $\mathcal{K}_0$, the index $i = 0$ is omitted. Likewise, for decompositions in the target frame $k = j$, the index k is omitted. Hence, $\boldsymbol{b}_1$ is equivalent ${}_0^1\boldsymbol{b}_1$.

Having measured the anthropometric distances d_{knee} and d_{ankle} between the knee joint center and the ankle joint center and the corresponding marker (see Fig. 11(b)), the following simple procedure is used to determine estimates of tibia and femur-fixed coordinate frames. By computing the distance between the ankle and the knee marker, the angle α between the connecting line of the tibia markers and the tibia joint centers is computed using the formula

$$\alpha = \arcsin \frac{d_{\mathrm{knee}} - d_{\mathrm{ankle}}}{d}. \tag{26}$$

With the unit direction vector $\boldsymbol{u}_{\mathrm{tibma}}$ of the line connecting the tibia markers, the axis direction of the knee- and the

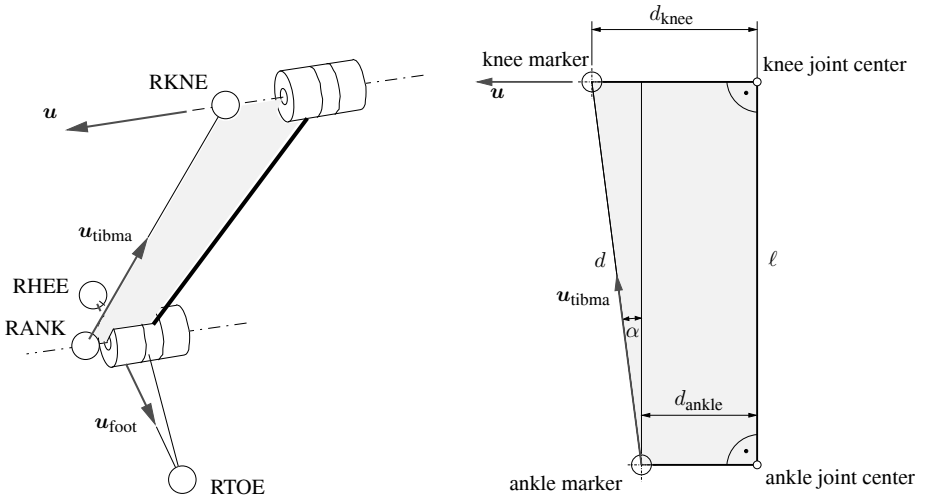

Fig. 11. Reconstruction of the knee joint axis: (a) direction of foot and tibia markers, (b) estimation of tibia joint centers.

ankle joint becomes

$$
\begin{aligned}
{}^0\boldsymbol{u} = \cos\alpha\, & \frac{{}^0\boldsymbol{u}_{\text{foot}} \times {}^0\boldsymbol{u}_{\text{tibma}}}{\| {}^0\boldsymbol{u}_{\text{foot}} \times {}^0\boldsymbol{u}_{\text{tibma}} \|} \\
& + \sin\alpha\, {}^0\boldsymbol{u}_{\text{tibma}}.
\end{aligned} \tag{27}
$$

Next, with ${}^0\boldsymbol{u}$ and the position ${}^0\boldsymbol{r}_{\text{knema}}$ of the knee marker, the location of the knee joint center is calculated as

$$
{}^0\boldsymbol{r}_{\text{knee}} = {}^0\boldsymbol{r}_{\text{knema}} - d_{\text{knee}}\, {}^0\boldsymbol{u}, \tag{28}
$$

and a coordinate system can be aligned with the femur by setting, using the position vector ${}^0\boldsymbol{r}_{\text{thima}}$ of the thigh marker:

$$
\begin{aligned}
{}^0\boldsymbol{e}_{3,\text{f}} &= {}^0\boldsymbol{u}, \\
{}^0\boldsymbol{e}_{1,\text{f}} &= \frac{({}^0\boldsymbol{r}_{\text{thima}} - {}^0\boldsymbol{r}_{\text{knee}}) \times {}^0\boldsymbol{u}}{\| ({}^0\boldsymbol{r}_{\text{thima}} - {}^0\boldsymbol{r}_{\text{knee}}) \times {}^0\boldsymbol{u} \|}, \\
{}^0\boldsymbol{e}_{2,\text{f}} &= {}^0\boldsymbol{u} \times {}^0\boldsymbol{e}_{1,\text{f}}.
\end{aligned}
$$

This leads to the rotation matrix

$$
{}^0\mathbf{R}_{\text{f}} = \left[{}^0\boldsymbol{e}_{1,\text{f}}\,,\, {}^0\boldsymbol{e}_{2,\text{f}}\,,\, {}^0\boldsymbol{e}_{3,\text{f}} \right] \tag{29}
$$

corresponding to the femur frame $\mathcal{K}_{\text{f}}$ displayed in Fig. 12.

For the estimation of the hip joint center, let the position of the femur head ($\equiv$ hip joint center) be given relatively to the femur frame $\mathcal{K}_{\text{f}}$ by the vector

$$
{}^{\text{f}}_{\text{f}}\boldsymbol{r}_{\text{hj}} = \begin{bmatrix} x_1 \\ x_2 \\ 0 \end{bmatrix} \tag{30}
$$

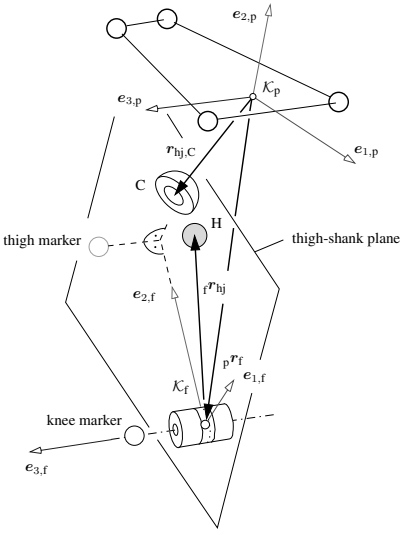

Fig. 12. Estimation of the hip joint center location in the thigh-shank plane.

which lies in the thigh/shank plane (see Fig. 12). The coordinates of the femur-fixed point H representing the hip joint center relative to the pelvis frame are

$$
{}^{\text{p}}_{\text{p}}\boldsymbol{r}_{\text{hj},i} = \mathbf{R}_i\, {}^{\text{f}}_{\text{p}}\boldsymbol{r}_{\text{f},i} + \mathbf{R}_{12,i}\, \boldsymbol{x}, \tag{31}
$$

where $\mathbf{R}_i = {}^{\text{p}}\mathbf{R}_{\text{f},i}$ is the rotation matrix between the estimated pelvis frame $\mathcal{K}_{\text{p}}$ and the estimated femur frame $\mathcal{K}_{\text{f}}$ at time t_i. Likewise, $\mathbf{R}_{12,i}$ is the matrix of the first two columns of $\mathbf{R}_i$ and $\boldsymbol{x} = [\, x_1\,,\, x_2\,]^{\text{T}}$. The position of the femur frame relative to the pelvis frame at time t_i is given

by ${}^{\mathrm{f}}_{\mathrm{p}}\boldsymbol{r}_{\mathrm{f},i}$. According to the "center transformation technique" (Ehrig *et al*., 2006), the coordinates x_1 and x_2 are chosen such that the squared norm of errors

$$\mathrm{f}(\boldsymbol{x}) = \sum_{i=1}^{m} ({}^{\mathrm{p}}_{\mathrm{p}}\boldsymbol{r}_{\mathrm{hj},i} - {}^{\mathrm{p}}_{\mathrm{p}}\boldsymbol{r}_{\mathrm{hj,C}})^2 \tag{32}$$

between the points H_i of this trajectory and their centroid C (visualized as "cup" in Fig. 12),

$${}^{\mathrm{p}}\boldsymbol{r}_{\mathrm{hj,C}} = \frac{1}{m}\sum_{i=1}^{m} (\mathbf{R}_i \, {}^{\mathrm{f}}_{\mathrm{p}}\boldsymbol{r}_{\mathrm{f},i} + \mathbf{R}_{12,i}\,\boldsymbol{x}), \tag{33}$$

is minimized over all m measured poses summing over $i = 1, \ldots, m$. By summing up and factoring out $\boldsymbol{x}$, one obtains

$${}^{\mathrm{p}}\boldsymbol{r}_{\mathrm{hj,C}} = \boldsymbol{a} + \mathbf{B}\,\boldsymbol{x}, \tag{34}$$

with $\boldsymbol{a}$ and $\mathbf{B}$ being constant. The first-order conditions for the optimum become

$$\begin{aligned}\frac{\partial \mathrm{f}}{\partial \boldsymbol{x}}(\boldsymbol{x}) = \sum_{i=1}^{m} (\mathbf{R}_{12,i} - \mathbf{B})^{\mathrm{T}} \big[(\mathbf{R}_i \, {}^{\mathrm{f}}_{\mathrm{p}}\boldsymbol{r}_{\mathrm{f},i} - \boldsymbol{a}) \\ + (\mathbf{R}_{12,i} - \mathbf{B})\,\boldsymbol{x} \big], \\ = \boldsymbol{a}_1 + \mathbf{B}_1\,\boldsymbol{x} = \mathbf{0},\end{aligned} \tag{35}$$

with obvious abbreviations $\boldsymbol{a}_1$ and $\mathbf{B}_1$, leading to the optimal point

$$\boldsymbol{x}^\star = -\mathbf{B}_1^{-1}\boldsymbol{a}_1. \tag{36}$$

When choosing the position of the hip joint relative to the femur frame as

$${}^{\mathrm{f}}_{\mathrm{f}}\boldsymbol{r}^\star_{\mathrm{hj}} = \begin{bmatrix} x_1^\star \\ x_2^\star \\ 0 \end{bmatrix}, \tag{37}$$

the fluctuations of the hip joint center with respect to the pelvis frame are minimized. This vector and the positions of the hip joint relatively to the pelvis frame are used to define the segment lengths of an open-chain kinematic model of the leg such as that described in (Kecskeméthy *et al*., 2003). The joint coordinates of the hip joint are obtained from the relative rotation matrix ${}^{\mathrm{p}}\mathbf{R}_{\mathrm{f},i}$. After fitting the hip joints, the segment lengths of the shank and the joint coordinates in knee and ankle are computed analogously.

4. Fusion of motion and MRI data

In the opinion of the authors, the only way to obtain better results for motion analysis is to incorporate additional patient-specific parameters into the mechanical model. Such an integration of additional patient-specific information is described in the following based on an approach to data fusion between MRI segmented images and motion analysis. MRI has the advantage that it does not impose health burden on test persons. From the MRI bone segmentation information, patient-specific data such as bone lengths, joint axis parameters, positions of bone landmarks (e.g., muscle insertion points), and other parameters can be obtained. Such segmentation techniques for MRI data have been presented recently (Cuypers *et al*., 2008), yielding quite good, although scattered results. After the segmentation of a bone from the MRI images, one obtains the surface as a scatter plot (see Fig. 13(a). From this scatter plot it is possible to obtain patient rough specific data directly (Tang *et al*., 2008). On the other hand, it is possible to fit superquadrics into the scatter plot, giving much more precise locations and properties functional entities, such as the femur head (see Fig. 13(b). Such techniques have been developed recently for recognition of further features, such as femur shaft, condyles, etc. (Cuypers, 2008).

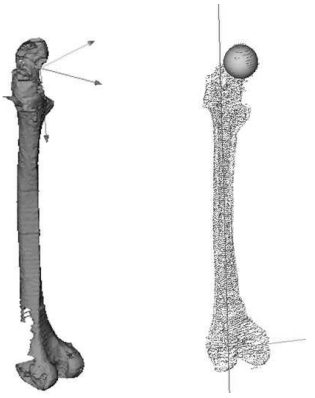

(a) b)

Fig. 13. Femur segmentation and fitting: (a) scatter plot, (b) super-quadric fitting.

Based on these functionalities and their data fusion with the measured motion data, an improved kinematical model of the human gait can be obtained, as described below.

4.1. Functional parameters of the pelvis. The functional landmarks at the pelvis are (see Fig. 14): 1—right hip joint center, 2—left hip joint center, 3—right spina iliacae anterior superior, 4—left spina iliacae anterior superior, 5—right spina iliacae posterior superior, and 6-left spina iliacae posterior superior. Using the landmarks 3–6 at the spina iliacae, the position of the pelvis frame $\mathcal{K}_{\mathrm{p}}$ can be calculated.

4.2. Functional parameters of the femur. The functional landmarks for the femur are (see Fig. 15): 1—femur

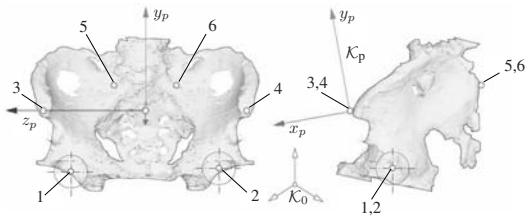

Fig. 14. Functional parameters of the pelvis.

axis, 2—center of the femur ball, 3—position of the tip of the trochanter major, 4—smallest diameter of the marrow array, 5—knee axis, 6—lengths a and b of the major and minor axis of the ellipse inscribed by the condyle area, respectively, 7—smallest diameter of the femoral neck, and 8—center point between the condyles. The most important functional parameters of the femur are the position of the femoral head and the knee axis. Additionally, some parameters for a computer aided prosthesis planning are obtained such as the position of the tip of the trochanter major, the smallest diameter of the marrow array and the diameter of the femoral neck. The femur fixed frame K_{f} is placed with its origin in the center of the femur ball with the z_f-axis parallel to the knee axis and the x_f-axis is normal to the plane through the knee axis and the center of the femur ball.

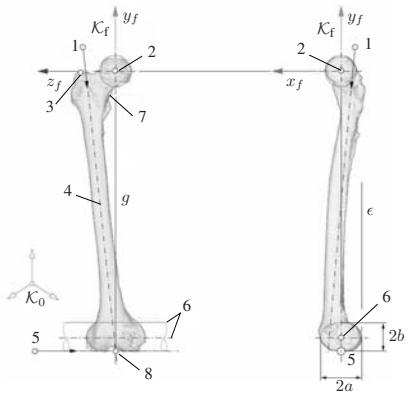

Fig. 15. Functional parameters of the femur.

4.3. Functional parameters of the shank (tibia and fibula). Because of the small movements between tibia and fibula, these two bones can be treated as one segment for normal gait-analysis problems. For the shank, the following functional parameters are identified (see Fig. 16): 1—tibia axis, 2—knee axis, 3—axis of the cylinder of the approximated upper ankle joint, and 4—radius and center of the upper ankle joint cylinder. The tibia-fixed frame K_{t} is located with its origin in the intersection between the axis of the tibia (1) and the knee axis (2).

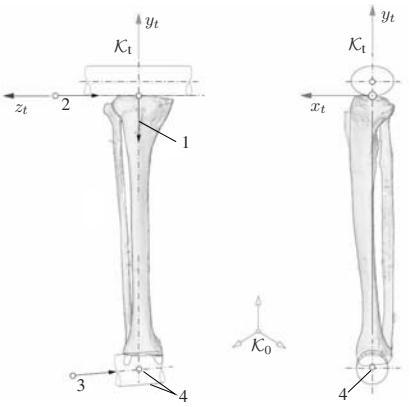

Fig. 16. Functional parameters of the tibia.

4.4. Functional parameters of the foot. The functional parameters of the foot are (see Fig. 17): 1—axis of the cylinder of the upper ankle joint, 2—radius and center of the upper ankle joint cylinder, 3—axis in between hind and mid feet, 4—axis in between mid and fore feet, 5—contact point of the hind foot, 6—medial contact point of the fore foot, and 7—lateral contact point of the fore foot. The frame of the foot is located at the center point of the axis of the upper ankle joint with the z_{foot}-axis aligned with the axis of the upper ankle joint. The contact points (5–7) are used to calculate the ground reaction forces (Liu *et al.*, 2008).

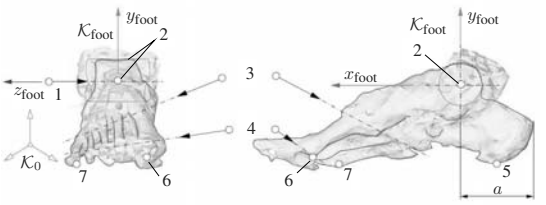

Fig. 17. Functional parameters of the foot.

4.5. Results. Using the patient-specific features described above, one can improve the quality of the model described in Section 3. To this end, blending techniques using Gaussian error interpolation can be used to interpolate between the motion capturing model and the geometrical MRI model (Tändl *et al.*, 2008). As a result, one obtains more accurate models of human gait. As an example of the application of such a technique. Fig. 18 shows the resulting relative rotations at the knee, i.e., between femur

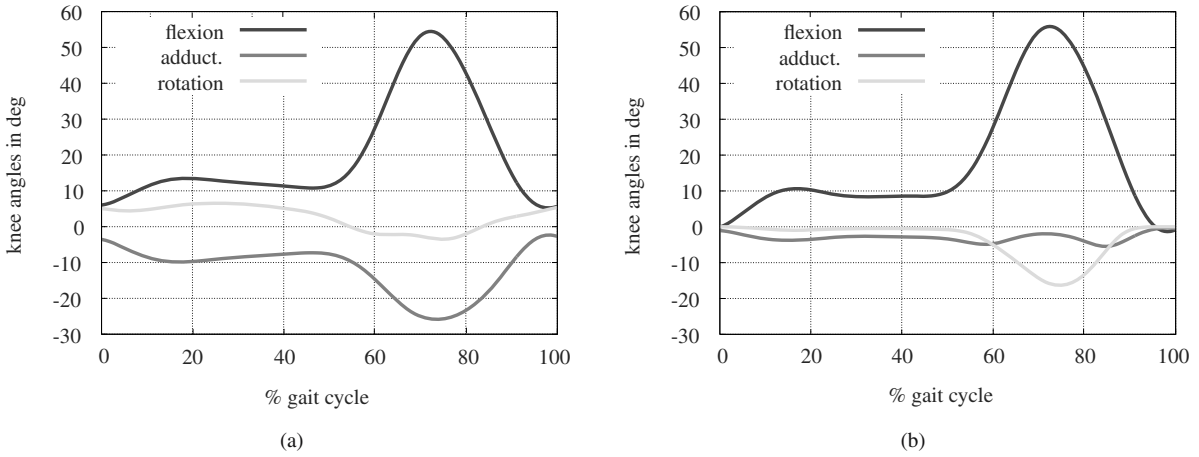

Fig. 18. Comparison of the knee angles (right leg) for Vicon's *Plug-in-Gait* and present kinematical model with MRI data fusion: (a) Vicon's *Plug-in-Gait* model, (b) present kinematical model with MRI data fusion.

and shank during a full gait both for the Vicon's *Plug-in-Gait* model and the present kinematical model with MRI data fusion. Here, positive angles are introduced as proper flexion for positive flexion angles, internal rotation for positive rotation angles, and varus rotation for positive adduction angles. It is clearly seen that the flexion and extension rotation, as the primary rotation of the knee, is basically equal for both cases. This shows that the main knee rotation is reproduced quite well independently of marker artifacts. On the other hand, one can clearly recognize that for the secondary adduction/abduction rotation, the *Plug-in-Gait* model renders quite unrealistic values, which can be drastically reduced using the new model. Here, the adduction angle remains slightly in valgus configuration, which is plausible due to the test person physiognomy. Moreover, the present kinematical model also reduces, during the stance phase, the second secondary knee angle, i.e., the rotation angle, while, during the swing phase, a slight external rotation is predicted by the new model, which is plausible as a compensation of pelvic rotation. In summary, a substantial improvement in knee and ankle axis prediction can be obtained, showing that more involved kinematical models may help to reduce motion capturing errors. These results can be still improved by employing better local models for knee and ankle, which is a topic to be analyzed in the future.

5. Validation

In order to validate the presented model, measurements with additional markers that are as close to the tibia as possible were carried out. Instead of using bone pins, which are very painful and which thus distort natural gait, a device was developed which could be attached quite rigidly to the tibia (see Fig. 19). The device consists of a concave metal plate which wraps around the anterior crest of the tibia and is fixed to it by an elastic strap. On the curved metal plate, a bow is attached which holds two markers RTIBM1 and RTIBM2 (shown here for the right leg). By this device, the motion of the markers RTIBM1 and RTIBM2 are quite close to the tibia and thus reduce skin motion artifacts with respect to the tibia. Moreover, an additional marker RTIBM3 was placed directly on the skin above the anterior crest near the foot at the medial side.

Using the three new tibia markers described above, a tibia-fixed coordinate frame can be generated in which the x-axis passes through the markers RTIBM1 and RTIBM2 and the xy-plane contains the markers RTIBM1, RTIBM2 and RTIBM3. By using this plane, small skin motions of the marker RTIBM3 have practically no influence on the frame position as they take place mainly in the xy-plane, which thus remains invariant to such relative motions. Apart from the new tibia-fixed frame just described, two further reference frames were constructed according to the approach of Vicon's *Plug-in-Gait* and the present approach (*MobileBody*). In Fig. 20, the average position fluctuations of the different markers are displayed for the three reference frames described above. On the one hand, one clearly recognizes the large fluctuations that the markers RTIBM1, RTIBM2 and RANKM (right ankle medial) undergo with respect to the *Plug-in-Gait* frame, showing that this frame performs large motions with respect to the tibia and thus generates spurious rotations. On the other hand, one can see that the present kinematical model (*MobileBody*) helps to reduce these fluctuations significantly, providing a better estimate of the tibia location from marker measurement. Another significant result from Fig. 20 is that both knee markers RKNE and RKNEM display strong fluctuations with respect to all reference frames, showing that the knee markers are not so well suited as a reference point for reproducing tibia motion. Additional verification procedures for quality as-

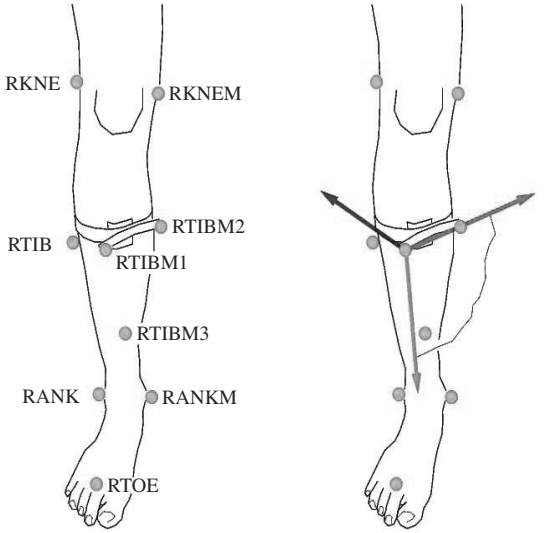

Fig. 19. Tibia fixed marker model.

sessment of the model can be carried out using methods of automatic verification, as presented in the paper (Auer and Luther, 2008), for which the cooperation is gratefully acknowledged.

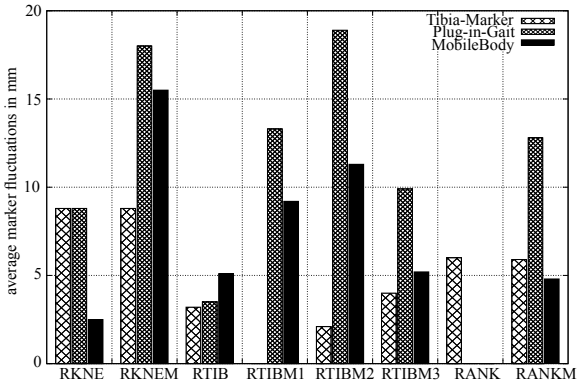

Fig. 20. Comparison of marker fluctuations for the different models.

6. Conclusions

Presented in this paper was a novel object-oriented model of human gait which can be used for improved accuracy reproduction of the motion of lower extremities. The simulation environment, termed *MobileBody*, is based on the general C++ multibody library MOBILE and thus offers an open architecture that is suitable to couple it to arbitrary sensor devices as well as 3D rendering techniques.

The described kinematical model allows one to build up the motion of the legs by starting at the feet and proceeding to the hip joints, where a kinematic closure condition is formulated. In this way, more exact bony motion reconstruction is possible, as shown in respective simulations and validation runs. In standard gait analysis, the model avoids huge, unrealistic internal/external rotations of the tibia and the femur, without requiring more markers than when using the *Plug-In-Gait* model. The model has been tested with several patients and is being currently employed to realize a full 3D simulation environment using head-mounted displays and clinically intuitive numeric scoring techniques.

Additional parameters from MRI data, such as muscle insertion points or bone landmarks (e.g., trochanter major), will help to improve the quality of the model and will lead to better results in the simulation of motion.

Acknowledgment

Funding by Projektträger Jülich, PtJ-Az.: z0608g02, project number 005-0608-0004, under financial support of the European Community (Europäischen Fonds für regionale Entwicklung EFRE), a thematic initiative of the Ministry of Innovation, Science, Research and Technology of the German State of North Rhine-Westphalia and in cooperation with Institut für Technologien der Biomechanik und Biomaterialien (ITBB), is gratefully acknowledged.

References

Auer, E. and Luther, W. (2008). Numerical verification assessment in computational biomechanics, *Proceedings of the Dagstuhl Seminar 08021: Numerical Validation in Current Hardware Architectures—From Embedded System to High-End Computational Grids, Dagstuhl Castle, Germany*, Lecture Notes in Computer Science, Springer, Berlin/Heidelberg, pp.145–160.

Barbour, N. and Schmidt, G. (2001). Inertial sensor technology trends, *IEEE Sensors Journal* **1**(4):332–339.

Cerveri, P., Pedotti, A. and Ferrigno, G. (2005). Kinematical models to reduce the effect of skin artifacts on marker-based human motion estimation, *Journal of Biomechanics* **38**(11): 2228–2236.

Cuypers, R. (2008). Functional bone reconstruction and manipulation in computer-aided surgery using superquadrics, *Proceedings of the 10th International Symposium Biomaterials: Fundamentals and Clinical Applications, Essen, Germany*.

Cuypers, R., Tang, Z., Luther, W. and Pauli, J. (2008). A parametrized model for efficient and accurate femur reconstruction using model-based segmentation and superquadric shapes, *Proceedings of the 4th International Conference on Telehealth and Assistive Technologies*, Baltimore, MD, USA, (accepted)

Davis, R. I., Õunpuu, S., Tyburski, D. and Gage, J. (1991). A gait analysis data collection and reduction technique, *Human Motion Science* **10**(5): 575–587.

Della Croce, U., Leardini, A., Chiari, L. and Cappozzo, A. (2005). Human movement analysis using stereophotogrammetry. Part 4: Assessment of anatomical landmark misplacement and its effects on joint kinematics, *Gait & Posture* **21**(2):212–225.

Delp, S. and Loan, J. (2000). A computational framework for simulating and analyzing human and animal movement, *IEEE Computing in Science and Engineering* **2**(5):46–55.

Ehrig, R. M., Taylor, W. R., Duda, G. N. and Heller, M. O. (2006). A survey of formal methods for determining the centre of rotation of ball joints, *Journal of Biomechanics* **39**(15): 2798–2809.

Hill, A. V. (1938). The heat of shortening and the dynamic constants of muscle, *Proceedings of the Royal Society London* **126**:136–195.

Kecskeméthy, A. and Hiller, M. (1994a). An object-oriented approach for an effective formulation of multibody dynamics, *Computer Methods in Applied Mechanics and Engineering* **115**(3–4): 287–314.

Kecskeméthy, A. and Hiller, M. (1994b). Object-oriented programming techniques in vehicle dynamics simulation, *Proceeding of the IMACS Symposium on Mathematical Modelling, Vienna, Austria*, Vol. 4, pp. 673–678.

Kecskeméthy, A., Lange, C. and Grabner, G. (2000). A geometric model for cylinder-cylinder impact with application to vertebrae motion simulation, *in* J. Lenarčič and M. M. Stanišić (Eds.), *7th International Symposium on Advances in Robot Kinematics, Piran-Portoroz, Slovenia,* Kluwer Academic Publishers, Dordrecht/Boston/London, pp. 345–354.

Kecskeméthy, A., Stolz, M., Strobach, D., Saraph, V., Steinwender, G. and Zwick, B. (2003). Improvements in measure-based simulation of the human lower extremity, *Proceedings of the IASTED Conference on Biomechanics, Rhodes, Greece*, pp. 155–160.

Kecskeméthy, A. and Weinberg, A. (2003). An improved elastokinematic model of the human forearm for biofidelic medical diagnosis, *CD Proceedings of the International ECCOMAS Thematic Conference on Advances in Computational Multibody Dynamics, Lisbon, Portugal*.

Liu, X., Kecskeméthy, A. and Tändl, M. (2008). A self-stabilized foot-ground contact model using two segments and cylinder-plane pairs, *i-FAB Congress, Bologna, Italy*.

Maestri, G. (1995). Capturing motion, *Computer Graphics World* **18**(12): 47–51.

Oxford Metrics, L. (2004). *Vicon Clinical Manager's User Manual*, Oxford Metrics Ltd.

Parenti-Castelli, V., Leardini, A., Di Gregorio, R. and O'Connor, J. (2004). On the modeling of passive motion of the human knee joint by means of equivalent planar and spatial parallel mechanisms, *Autonomous Robots* **16**(2): 219–232.

Peters, A., Sangeux, M., Morris, M. and Baker, R. (2009). Determination of the optimal locations of surface-mounted markers on the tibial segment, *Gait & Posture* **29**(1): 42–48.

Piazza, S. J. and Cavanagh, P. R. (2000). Measurement of the screw-home motion of the knee is sensitive to errors in axis alignment, *Journal of Biomechanics* **33**(8): 1029–1034.

Stroustrup, B. (1991). *The C++ Programming Language, Second Edition*, Addison-Wesley Series in Computer Science, Addison-Wesley Publishing Company, Reading, MA.

Tändl, M., Stark, T., Erol, N., Löer, F. and Kecskeméthy, A. (2008). An integrated simulation environment for human gait analysis and evaluation, *Proceedings of the 10th International Symposium on Biomaterials: Fundamentals and Clinical Applications, Essen, Germany*.

Tang, Z., Pauli, P. D. J. and Kecskeméthy, P. D. A. (2008). Automatic identification of functional kinematic bone features from mrt segmentation for gait analysis, *Proceedings of the 10th International Symposium on Biomaterials: Fundamentals and Clinical Applications, Essen, Germany*, (submitted).

Vicon Motion Systems Limited (2007). *Plug-in-Gait Marker Placement—Documentation*, Available at: `http://www3.uta.edu/faculty/ricard/Grad%20Biomech/Vicon%20Manuals/`.

Winter, D. (1990). *Biomechanics and Motor Control of Human Movement, 2nd Edn.*, John Wiley & Sons Inc., New York, NY.

Wirfs-Brock, R. and Wilkerson, B. (1989). Object-oriented design: A responsibility-driven approach, *Proceedings of the Conference on Object-Oriented Programming Systems, Languages and Applications. New Orleans, LA, USA,* pp. 71–75.

Zordan, V. B. and Van Der Horst, N. C. (2003). Mapping optical motion capture data to skeletal motion using a physical model, *Proceedings of the Eurographics/SIGGRAPH Symposium on Computer Animation, San Diego, CA, USA*, pp. 245–250.

Martin Tändl received the Dipl.-Ing. degree in mechanical engineering from the Graz University of Technology, Austria, in 2001. In 2002, he worked as a scientific assistant at the Chair of Mechanics and Mechanisms at the Graz University of Technology and from 2002 to 2008 as a scientific assistant at the Chair of Mechanics and Robotics at the University of Duisburg-Essen, Germany. His research interests include the kinematics of spatial guided motion, multibody dynamics, and biomechanics.

Tobias Stark studied technical computer science at the Technical University of Berlin, Germany. He received his Dipl.-Ing. degree in 2006. From 2002 to 2006, he worked as a research student at Daimler AG (automotive industry). Since 2007, he has been working as a scientific assistant at the Chair of Mechanics and Robotics at the University of Duisburg-Essen, Germany. His research interests focus on biomechanics, robotics, and virtual reality.

Nihat Ercümet Erol studied human medicine from 2000 till 2006 at the medical school of Ruhr-Universität Bochum, Germany. After passing his medical exam in 2006, he worked as a physician in the orthopaedic surgery centre at St. Anna Hospital in Herne, Germany. Since 2008 he has been employed as a scientific assistant and physician at the Department of Orthopaedic Surgery at the University Hospital Essen, Germany. His research interests include the biomechanics of humans, gait analysis, endoprosthetics, and the research of serve trauma patients/polytrauma.

Franz Löer is a director of the Orthopaedic Clinic of the University Hospital Essen, Germany. His research interests include artificial joints and total joint arthroplasty, rheumatology, spine diseases, paediatric orthopaedics, bone tumours, arthroscopic surgery, foot and ankle surgery, as well as septic surgery of the locomotor system.

Andrés Kecskeméthy graduated from the University of Stuttgart in mechanical engineering in 1984 and received his Ph.D. in mechanical engineering from the University of Duisburg in 1993. From 1994 to 1995, he stayed as a senior guest researcher at the Centre for Intelligent Machines at McGill University. In 1996, was appointed a professor at the Technical University of Graz, where he held the Chair for Mechanics until 2002. In 2002, Professor Kecskeméthy moved to the University of Duisburg-Essen, where he holds the Chair for Mechanics and Robotics at the Institute of Mechatronics and System Dynamics. He has worked in the areas of the kinematics and dynamics of multibody systems. His current research interests lie in the areas of biomechanics and computer-based surgery planning, virtual reality, and heavy-weight robotics.

Received: 10 September 2008
Revised: 9 February 2009